

## **Numerical Simulation of Fluid and Heat Transfer in a Biological Tissue Using an Immersed Boundary Method Mimicking the Exact Structure of the Microvascular Network**

**Yuanliang Tang<sup>1,2</sup>, Lizhong Mu<sup>1</sup> and Ying He<sup>1,\*</sup>**

**Abstract:** The aim of this study is to develop a model of fluid and heat transfer in a biological tissue taking into account the exact structure of the related microvascular network, and to analyze the influence of structural changes of such a network induced by diabetes. A cubic region representing local skin tissue is selected as the computational domain, which in turn includes two intravascular and extravascular sub-domains. To save computational resources, the capillary network is reduced to a 1D pipeline model and embedded into the extravascular region. On the basis of the immersed boundary method (IBM) strategy, fluid and heat fluxes across a capillary wall are distributed to the surrounding tissue nodes by a delta function. We consider both steady and periodic blood pressure conditions at the entrances of the capillary network. Under steady blood pressure conditions, both the interstitial fluid pressure and tissue temperature around the capillary network are larger than those in other places. When the periodic blood pressure condition is considered, tissue temperature tends to fluctuate with the same frequency of the forcing, but the related waveform displays a smaller amplitude and a certain time (phase) delay. When the connectivity of capillary network is diminished, the capacity of blood redistribution through the capillary network becomes weaker and a subset of the vessel branches lose blood flow, which further aggravates the amplitude attenuation and time delay of the skin temperature fluctuation.

**Keywords:** Bioheat transfer, porous media, immersed boundary method, diabetes, microvascular dysfunction, skin temperature fluctuation.

### **1 Introduction**

Many diseases, including diabetes and hypertension, are accompanied with microangiopathy. Hemodynamic changes of subcutaneous microcirculation can be reflected in the variations

---

<sup>1</sup> Key Laboratory of Ocean Energy Utilization and Energy Conservation of Ministry of Education, Dalian University of Technology, Dalian, 116024, China.

<sup>2</sup> National Engineering Research Center for Healthcare Devices, Guangdong Key Lab of Medical Electronic Instruments and Polymer Material Products, Guangdong Institute of Medical Instruments, Guangzhou, 510500, China.

\* Corresponding Author: Ying He. Email: heying@dlut.edu.cn.

Received: 28 March 2019; Accepted: 12 October 2019.

of skin temperature, thus monitoring subcutaneous blood flow is possible via thermal methods. Indirect blood flow detection by thermal method can be categorized into two subclasses: the method based on the information of absolute skin temperature and that based on the fluctuation characteristics of skin temperature. Compared with the former, thermal fluctuation method can provide more targeted information for functional monitoring of microcirculation since it is not easy to be affected by the environmental factors.

Recently, high attentions have been paid to the study of spontaneous fluctuations of microvessels. Bracic et al. [Bracic and Stefanovska (1998)] found through experimental analysis that the spontaneous fluctuations of microvessels were related to the following activities: cardiac, respiratory, myogenic, neurogenic and endothelial regulations, which have distinct regulating periods. Meanwhile, skin temperature fluctuations have been proved to correlate with vascular tone regulations [Sagaidachnyi, Skripal, Fomin et al. (2014)] and can be a tracer of the status of subcutaneous blood flow [Frick, Mizeva and Podtaev (2015)]. A spectral filtering approach [Sagaidachnyi, Fomin and Usanov (2017)] has been developed to use thermal imaging as a tool for the evaluation of peripheral haemodynamics. In recent decades thermal fluctuation method has been gradually applied to clinical studies. For example, it is reported that skin temperature fluctuation amplitudes become much smaller in contralateral cooling [Smirnova, Podtaev, Mizeva et al. (2013)] and local heating [Parshakov, Zubareva, Podtaev et al. (2017)] tests, indicating endothelium-dependent vasodilation dysfunctions in diabetes.

However, the reasons for the weakening fluctuation characteristics of skin temperature in diabetes as mentioned above are still not very clear. According to the theory of thermal wave propagation, it is known that fluctuation amplitude attenuates and phase shift increases with the increasing of the propagation length. In addition, fluctuation frequency and tissue thermal conductivity also have influence on thermal wave propagation [Tang, Mizeva and He (2016)]. Thermo-fluid modeling may contribute to the analysis of the relationship between microangiopathy and the variation of skin temperature fluctuation. In 1948, Pennes [Pennes (1948)] proposed the bioheat transfer equation (BHTE) according to the measured temperatures of tissue and blood at the forearm, which has proven to be a key underlying basis for modeling heat transport in biological tissue. In BHTE, it is assumed that microvessels are uniformly distributed in biological tissue, and complete heat exchange occurs between blood and the surrounding tissue. The blood acts as a heat source or sink. As blood leaves the capillary bed, it has become complete thermal equilibration with the surrounding tissue and enters the venous circulation at this temperature. Despite the extensive use of BHTE in the computation of regional organ's or whole body's temperature, it cannot describe accurately the heat transfer phenomenon of local tissue in a small scale with a real structure of vessel network in tissue. Thus, in modeling human thermo-regulation [Dang, Xue, Zhang et al. (2018), Tang, He, Shao et al. (2016), Salloum, Ghaddar and Ghaliour (2007)] or the effect of hyperthermia induced by heating magnetic nanoparticles [Astefanoaei, Dumitru and Stancu (2014)], heat transfer inside larger vessels and tissue are frequently taken into account separately. Local blood temperatures are obtained from the computation of fluid dynamics and are assigned as the boundary conditions in using BHTE.

After the BHTE was proposed, some revised models were successively developed in recent decades, such as Wulff [Wulff (1974)], Klinger [Klinger (1974)] and Weinbaum et al. [Jiji, Weinbaum and Lemons (1984)]'s model. However, the complexities of these models limit their further development and wider applications. An alternative approach is to regard biological tissue as a porous media, and to analyze the tissue heat transfer characteristics by porous medium theory. This approach needs less parameters in the process of modeling compared with other heat transfer models, which are adopted in the models of Xuan et al. [Xuan and Roetzel (1997)], Yuan et al. [Yuan, Yang and Liu (2014)], and Nakayama et al. [Nakayama and Kuwahara (2008)].

Multiscale modeling method is frequently applied in simulations of hemodynamics, where blood flow in the capillary network is assumed as 1D flow since the 3D feature of the blood flow inside capillaries is not remarkable. A lot of work about multiscale modeling for microcirculation and interstitial flow in solid tumor can be found [Pozrikidis (2010), Cattaneo and Zunino (2014), Shipley and Chapman (2010)]. In coupling the interplay between blood flow and interstitial fluid flow, immersed boundary method (IBM) is commonly used. IBM was originally developed for analyzing cardiac hemodynamics by Peskin [Peskin (1972)]. Since it is much simpler in handling the complex and moving geometries and with good parallelism, nowadays it has been widely applied in solving problems of fluid-structure interactions with moving boundaries. Particularly, the coupling of IBM with lattice Boltzmann method has been proved to be high efficiency with much stability in the simulation of moving boundary problems, such as insect hovering motion [Gao and Lu (2008)], fish swimming [Tian, Luo, Zhu et al. (2011)], particle sorting in a determined lateral displacement device [Wei, Song, Shen et al. (2015)] and the motion and deformation of red blood cell [Hassanzadeh, Pourmahmoud and Dadvand (2017), Ghafouri1 and Hassanzadeh (2017)]. Recently, an improved IB-LBM method was presented by including cubic spline interpolation to give a smoother shape of red blood cell for every step of coupling [Hassanzadeh, Pourmahmoud and Dadvand (2019)]. Liu et al. [Liu, Kim and Tang (2007)] developed immersed finite element method (IFEM) by extending IB method, where the fluid spans over the entire computational domain with an Eulerian mesh and a Lagrangian solid mesh is generated on the top of the Eulerian fluid mesh. The advantage of this method is the solid part can be considered as a continuum rather than an immersed boundary layer.

IBM is not only applied in solving the moving boundary problems but also in mass transport problems. The vasomotion of arteriolar wall induced by myogenic response can be well modeled by using IB [Arthurs, Moore, Peskin et al. (1998)]. Wei et al. [Wei, Mu and Tang (2019)] successfully simulated the influence of red blood cell on nitric oxide distribution in a microvessel using immersed boundary method. Cattaneo et al. [Cattaneo and Zunino (2014)] developed a computational model for fluid exchange between microcirculation and tissue interstitium, where the capillaries and interstitial volume were described as two independent structure and IBM was adopted to couple the 1D flow through the network and 3D flow through the interstitial volume. To the best of the authors' knowledge, this kind of modeling strategy hasn't been applied in solving heat transfer problems in complex structures.

In this paper, the objectives of this study are to develop a model of fluid and heat transfer in biological tissue containing exact microvascular network structure, and to analyze the influence of structural changes of the network in diabetes on flow and heat transfer. The interplay between blood flow in capillary network and interstitial volume was considered by using IBM. Tissue temperature distribution and fluctuation characteristics caused by subcutaneous blood flow were investigated; then the influence of structural alterations of microvasculature on thermal wave propagation was further analyzed.

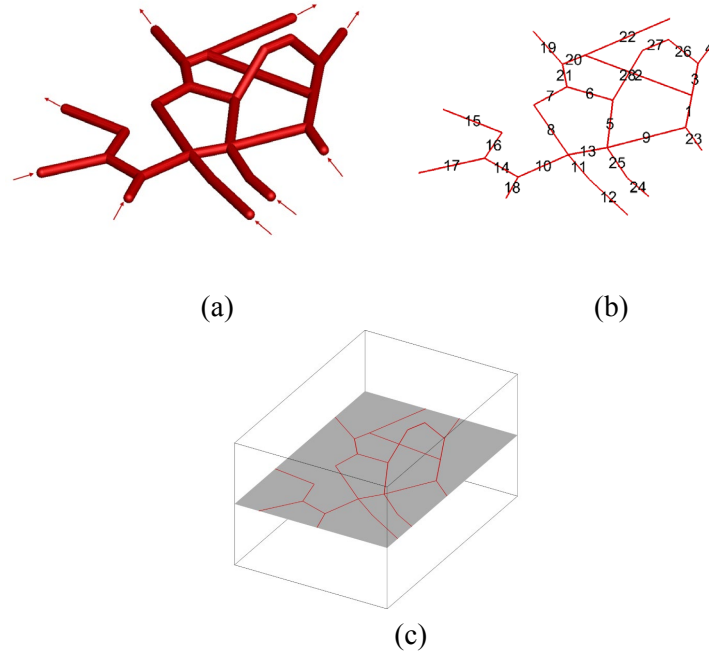


**Figure 1:** Geometrical model for the (a) 3D capillary network, (b) 1D capillary network indexed by numbers, and (c) 3D tissue with the capillary network

## 2 Methods

### 2.1 Geometrical modeling of capillary network and the surrounding tissue

A capillary network [Secomb (1993)] derived from rat's subcutaneous tissue was used in our study. As shown in Fig. 1(a), the network consists of 28 capillary branches, including five entrance branches and four exit branches. To reduce computational costs, we simplified the network to a 1D model, then embedded it into a cubic tissue region, as shown in Figs. 1(b) and (c). The 1D model of blood flow refers that the blood flow in each single vessel is governed by Poiseuille equation and the flow at the bifurcation satisfies the continuity condition. By combining the Poiseuille equation and boundary conditions at the bifurcation points, the pressure within the whole capillary network can be solved. The tissue is with the size of  $370 \times 250 \times 200 \mu\text{m}$ , of which every capillary element has its own diameter, length and three-dimensional space coordinates. Most of the branches are located in the mid-plane of the tissue region except one branch with 3D coordinates.

**2.2 Mathematical modeling for flow and heat transfer**

In using Pennes equation to deal with bioheat transfer problem, blood perfusion is the most important parameter to be determined. However, when microvasculature is altered, it will not be easy to determine the value definitely. Thus, fluid and heat transfer in biological tissue containing the structure of microvascular network may be an alternative which can give the influence of blood flow with different vasculature. In the modeling work, the most innovative point is using IBM to couple heat transfer in blood and fluid flow in different domains. Then the flow in the capillary network and interstitial tissue can be considered respectively. In capillaries, blood flow can be described as laminar stationary flow of incompressible viscous fluid through a cylindrical tube. According to Poiseuille’s law, blood flow rate can be computed by:

$$\mathbf{u}_b = -\frac{R^2}{8\mu} \frac{\partial P_b}{\partial s} \boldsymbol{\lambda} \tag{1}$$

where  $\mathbf{u}_b$  is blood flow rate,  $P_b$  is blood pressure,  $\mu$  is blood dynamic viscosity,  $R$  is capillary radius.  $\boldsymbol{\lambda}$  is the orientation of a branch in the capillary network. The interstitial tissue region can be treated as isotropic porous medium with interstitial fluid and solid tissue, so the fluid flow and heat transfer phenomenon can be described by porous medium theory. According to Darcy’s law, interstitial fluid seepage velocity can be computed by:

$$\mathbf{u}_t = -\frac{k}{\mu} \nabla P_t \tag{2}$$

where  $\mathbf{u}_t$  is interstitial fluid flow rate,  $P_t$  is interstitial fluid pressure,  $k$  is fluid permeability, and  $\mu$  is dynamic viscosity of the interstitial fluid. If interstitial fluid and tissue cells reach a thermal equilibrium, the coupled energy equation can be written as:

$$(\rho c)_t \frac{\partial T_t}{\partial t} + (\rho c)_f \mathbf{u}_t \cdot \nabla T_t = \lambda_t \nabla^2 T_t + Q_t \tag{3}$$

where  $(\rho c)_t$ ,  $\lambda_t$  and  $Q_t$  are overall heat capacity per unit volume, overall thermal conductivity, and overall heat production per unit volume of the porous medium composed of fluid and solid tissue. They have the formulas as:

$$\begin{aligned} (\rho c)_t &= (1 - \varepsilon)\rho_s c_s + \varepsilon\rho_f c_f \\ \lambda_t &= (1 - \varepsilon)\lambda_s + \varepsilon\lambda_f \\ Q_t &= (1 - \varepsilon)Q_s + \varepsilon Q_f \end{aligned} \tag{4}$$

The subscripts  $f, s$  represent interstitial fluid and tissue cells, respectively.  $\varepsilon$  is the porosity of the tissue with the value of 0.3.  $T_t$  denotes the temperature of the porous tissue.

The fluid flow and heat transfer model must be complemented with appropriate boundary conditions. In our work, blood pressures at the entrance and exit of the network were given as follows:

$$P_b \Big|_{\text{entrance}} = P_{b,\text{in}}, P_b \Big|_{\text{exit}} = P_{b,\text{out}} \tag{5}$$

At the skin surface, normal gradient of blood pressure was set to be 0. At the other boundaries connected to the inner tissue, Robin-type boundary conditions were given. In these cases, the boundary conditions can be summarized as:

$$\begin{aligned} -\frac{k}{\mu} \frac{\partial P_t}{\partial x} \Big|_{x=0, 250 \mu\text{m}} = \beta_f (P_t - P_0), -\frac{k}{\mu} \frac{\partial P_t}{\partial y} \Big|_{y=0, 370 \mu\text{m}} = \beta_f (P_t - P_0) \\ -\frac{k}{\mu} \frac{\partial P_t}{\partial z} \Big|_{z=0} = \beta_f (P_t - P_0), -\frac{k}{\mu} \frac{\partial P_t}{\partial z} \Big|_{z=200 \mu\text{m}} = 0 \end{aligned} \quad (6)$$

where  $P_0$  is far field pressure,  $\beta_f$  is the effective permeability with respect to fluid transport. Regarding the temperature boundary conditions, convection and radiation occurred at the skin surface. At the other boundaries connected to the inner tissue, adiabatic boundary conditions were given as:

$$\begin{aligned} -\lambda_t \frac{\partial T_t}{\partial x} \Big|_{x=0, 250 \mu\text{m}} = 0, -\lambda_t \frac{\partial T_t}{\partial y} \Big|_{y=0, 370 \mu\text{m}} = 0 \\ -\lambda_t \frac{\partial T_t}{\partial z} \Big|_{z=0} = 0, -\lambda_t \frac{\partial T_t}{\partial z} \Big|_{z=200 \mu\text{m}} = h_{c,r} (T_t - T_\infty) \end{aligned} \quad (7)$$

where  $h_{c,r}$  is the sum of convective and radiative and heat transfer coefficient. When the air velocity is less than 0.15 m/s, the convective heat transfer coefficient is 4 W/m<sup>2</sup>K. At room temperature, the radiative heat transfer coefficient is almost constant and equals to 4.7 W/m<sup>2</sup>K. Since some part of fluid is across the capillary wall while blood flows through the capillary network, the blood plays as the heat source of the tissue as well. The heat flux from the blood to the surrounding tissue is determined by immersed boundary method.

### 2.3 Coupling of the two subdomains

When there is no fluid exchange occurring in capillary wall, the mass conservation equations for blood in capillary network and interstitial fluid can be written as:

$$\begin{aligned} \nabla \cdot \mathbf{u}_b = 0 \\ \nabla \cdot \mathbf{u}_t + L_p^{\text{LF}} (P_t - P_L) = 0 \end{aligned} \quad (8)$$

where  $L_p^{\text{LF}} (P_t - P_L)$  represents lymphatic drainage,  $L_p^{\text{LF}}$  is the effective coefficient of hydraulic conductivity of lymphatic wall,  $P_t$  is interstitial fluid pressure, and  $P_L$  is lymphatic fluid pressure, whose values were referred to the reference Cattaneo et al. [Cattaneo and Zunino (2014)]. It has been demonstrated that lymphatic drainage plays an important role in maintaining interstitial fluid pressure [Shipley and Chapman (2010)]. When lymphatic drainage is absent, excessive fluid in the interstitium may be only discharged though fluid exchange with exterior, which may cause tissue edema more easily. In fact, capillary walls are semi-permeable to blood. Fluid flux per unit surface across capillary wall can be computed by using Starling's law of filtration:

$$J_f = L_p (P_b - P_t) \quad (9)$$

where  $J_f$  is fluid flux,  $L_p$  is the permeability of capillary wall to fluid, which is set to 1.0E-12 m<sup>2</sup>s/kg. Heat exchange occurs between blood and interstitial tissue when blood

plasma permeates across the capillary wall. We assumed a complete thermal exchange occurred between them, and heat flux per unit surface across capillary wall can be computed by using  $J_f$  :

$$J_{\text{heat}} = \rho_f c_f J_f (T_b - T_t) \tag{10}$$

The 1D network can be regarded as a concentrated source immersed into interstitial tissue, thus fluid and heat flux per unit length along the circumference of capillary walls can be obtained by the following integral formulas:

$$f_f = \int_0^{2\pi} J_f R d\theta, f_{\text{heat}} = \int_0^{2\pi} J_{\text{heat}} R d\theta \tag{11}$$

For simplification of computing, the interstitial fluid pressures and tissue temperatures were averaged around the targeted capillary node, and the fluid and heat flux can be approximated as:

$$f_f \approx 2\pi R \overline{J_f} = 2\pi R L_p (P_b - \overline{P_t}), f_{\text{heat}} \approx 2\pi R \overline{J_{\text{heat}}} = 2\pi R \rho_f c_f \overline{f_f} (T_b - \overline{T_t}) \tag{12}$$

The spatial dimensions of the two sub-domains for the capillary network and interstitial tissue are not naturally matched since the space coordinates of the capillary network is complex. We applied IBM to couple the two sub-domains in the computation. In dealing with the problems of fluid-structure interaction, the interpolated bounce back (BB) scheme and immersed boundary method are frequently employed. The concept of BB is to compute the particle distribution function in an off-grid position by an interpolation function from the on-grid nodes, which has Eulerian nature [Mei, Yu, Shyy et al. (2002)]. Although it is with second-order accurate, it is not easy to be implemented, especially for a complex geometry. On the other hand, the immersed boundary method is simpler by using a delta function to couple the Lagrangian solid boundary with the fluid mesh. The numerical tests have proved that the IB method is more stable than the BB scheme [Rosis, Ubertini and Ubertini (2014)], In treating a fixed-boundary problem, there's no significant difference between BB and IB method and BB may be computational cheaper than IB. Considering the simplicity and the advantage in stability, IB method was employed in the work.

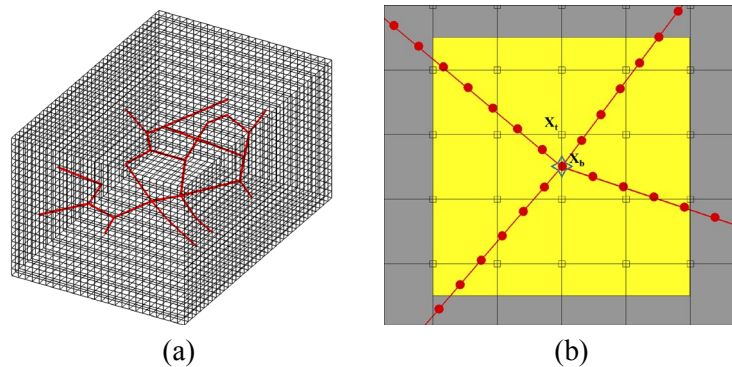


**Figure 2:** (a) Discretization strategy for the 3D model; (b) The coupling strategy between the vessel and the tissue nodes

First, two sets of separate grids were generated to discretize the two subdomains, as shown in Fig. 2(a); Then, fluid and heat flux were smoothly distributed to the adjacent tissue nodes using an approximate delta function:

$$F_f(\mathbf{x}_t) = \sum_b D(\mathbf{x}_t - \mathbf{x}_b) f_f(\mathbf{x}_b) \Delta s, F_{\text{heat}}(\mathbf{x}_t) = \sum_b D(\mathbf{x}_t - \mathbf{x}_b) f_{\text{heat}}(\mathbf{x}_b) \Delta s \quad (13)$$

where the approximate delta function  $D(\mathbf{x})$  can generally be written as:

$$D(\mathbf{x}) = \frac{1}{\Delta h^3} \Psi\left(\frac{x}{\Delta h}\right) \Psi\left(\frac{y}{\Delta h}\right) \Psi\left(\frac{z}{\Delta h}\right) \quad (14)$$

Here  $\Delta h$  is the grid size for the tissue domain. The selection of approximate delta function is of importance in IBM, which is related to the numerical accuracy and efficiency. For comparison, different interpolation kernels were tested, which are written as the following forms:

$$\Psi_1(r) = \begin{cases} \frac{1}{4} \left(1 + \cos \frac{\pi r}{2}\right), & |r| \leq 2 \\ 0, & |r| > 2 \end{cases} \quad (15)$$

$$\Psi_2(r) = \begin{cases} \frac{1}{8} (3 - 2r + \sqrt{1 + 4r - 4r^2}), & 0 \leq r \leq 1 \\ \frac{1}{8} (5 - 2r - \sqrt{-7 + 12r - 4r^2}), & 1 < r \leq 2 \end{cases}$$

The graph of the delta function  $\Psi_1$  in 2D domain is shown in Fig. 3(a). Meanwhile the comparison of  $\Psi_1$  and  $\Psi_2$  is given in Fig. 3(b) in 1D domain. It is seen that the profiles of the two functions are almost overlapped. Hence, in the simulation, the classical and widely used scheme of  $\Psi_1(r)$  was adopted. In addition, the ratio between the solid and fluid mesh size is crucial for the simulation. A too large one between Eulerian and Lagrangian mesh resolution may cause fluid leakage through the membrane, whereas a too small value may cause numerical “stick” [Krüger (2012)]. It is suggested that the value be smaller than 1/2 [Peskin (2002)] in order to avoid fluid leakage problem. Therefore, the ratio of the two mesh size is set to 1/2.

With considering fluid and heat exchange across capillary wall and lymphatic drainage, the mass conservation and energy equations are finally written as:

$$\begin{aligned} \pi R^2 \nabla \cdot \mathbf{u}_b &= -f_f \\ \nabla \cdot \mathbf{u}_t + L_p^{\text{LF}} (P_t - P_l) &= F_f \\ (\rho c)_t \frac{\partial T_t}{\partial t} + (\rho c)_f \mathbf{u}_t \cdot \nabla T_t &= \lambda_t \nabla^2 T_t + Q_t + F_{\text{heat}} \end{aligned} \quad (16)$$

An in-house FORTRAN program was developed to numerically solve the model by finite difference method (FDM). The steady blood flow field in the capillary network was solved first. Subsequently, the fluid and heat flux across the vessel walls were computed according to Eq. (12). Thus, the fluid and heat flux in the surrounding porous tissue nodes may be evaluated by using delta function. After the interstitial fluid velocity and heat

source transported from blood were determined, the tissue temperatures were finally computed according to the energy equation in Eq. (16).

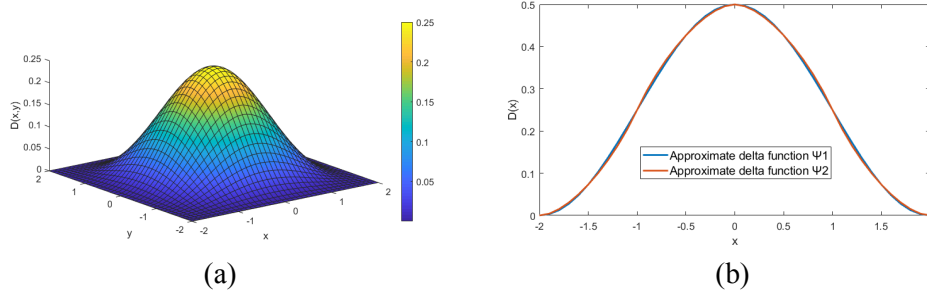


**Figure 3:** (a) The Dirac delta function in 2D domain; (b) the comparison of the two kind of delta functions in 1D domain

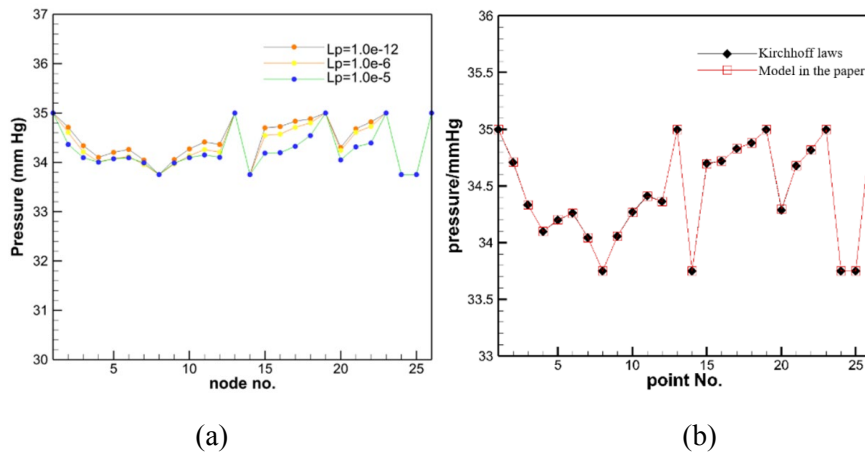


**Figure 4:** (a) Comparison of pressures in the network computed by Kirchhoff law and the numerical method; (b) Computed pressure variations under different permeability

### 3. Results

#### 3.1 Steady-state distributions of interstitial fluid flow and temperature fields

As the validation, we calculated blood pressure distribution in the network under the condition that capillary walls were non-permeable to blood, i.e., the permeability of capillary wall to fluid was set to 0. In this case, the capillary network is analogous to an electric circuit composed of series parallel-resistance elements, the exact solution of which can be obtained using Kirchhoff laws. According to the flow at the capillary level, the inlet pressure was set to 35 mmHg and the outlet pressure was set to 33.75 mmHg respectively. Pressures of branching nodes are plotted in Fig. 4(a), and we can see the simulated results by our model are almost the same as the exact solution. Furthermore, we tested the influence of wall permeability on blood pressure distribution along the capillary network. Three values of  $L_p$  were adopted with the same inlet and outlet

pressure. As shown in Fig. 4(b), the pressures of internal nodes are decreased with the increasing of  $L_p$ , which make sense since transmembrane transport of fluid leads to the reduce of fluid mass and pressure decreasing inside the capillaries.

After the validation, the steady-state distributions of interstitial fluid flow and temperature fields were obtained as shown in Fig. 5. It is seen that in the mid-plane of the tissue region, the interstitial fluid pressure, seepage velocity and tissue temperature decrease with the increasing of the distance from the capillary network. Around the capillary network, the seepage velocity vectors are almost perpendicular to the axis of each capillary branch. Although temperature difference exists between capillaries and the surrounding tissue, there is no significant distinction for the tissue temperature in the area far away from the capillaries.

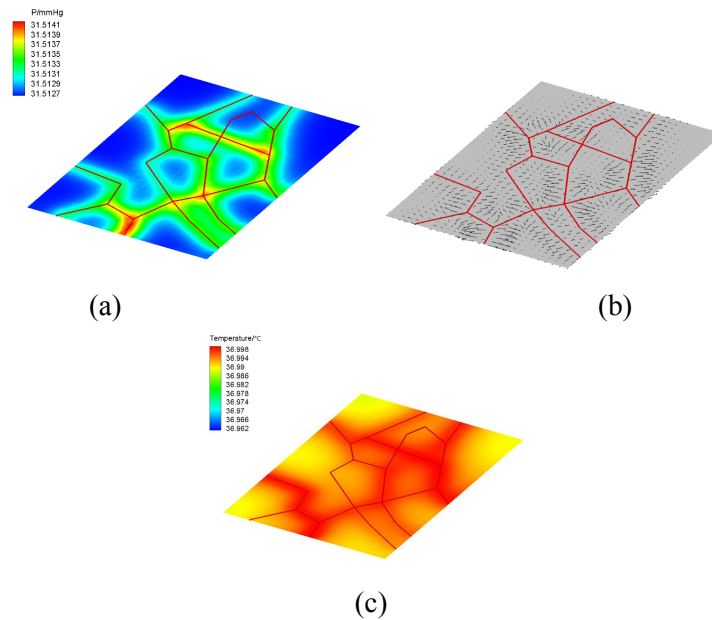


**Figure 5:** Steady-state distributions of interstitial fluid flow and temperature fields: (a) Interstitial pressure field; (b) Seepage velocity vector field; (c) Tissue temperature field

**Table 1:** Temperature fluctuation characteristics at different tissue nodes

Node	Fluctuation amplitude ( $\Delta T$ ), °C	Time delay ( $\Delta t$ ), s
X1	0.0031	4.5
X3	0.0026	6.9
X2	0.0019	7.2

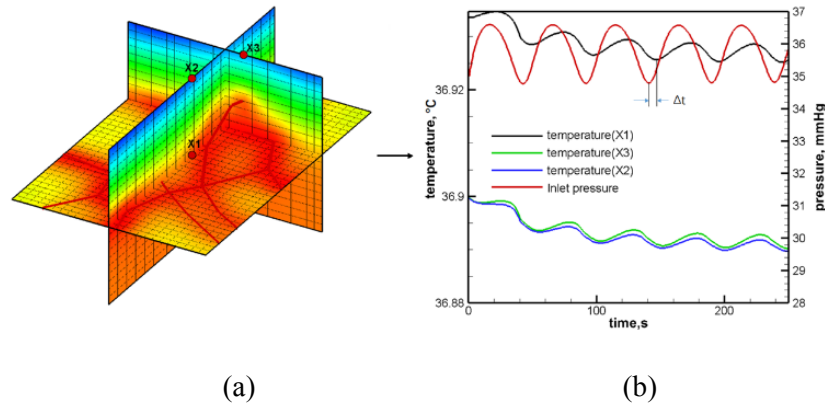


**Figure 6:** The influence of pulsatile blood pressure on tissue temperature field (a) tissue temperature distribution in the 3D domain; (b) Variations of inlet blood flow pressure and temperatures at the three indexed points

**3.2 The influence of pulsatile blood pressure on tissue temperature field**

To simulate thermal wave propagation phenomenon in tissue, pulsatile inlet pressure was set at the five entrances of the capillary network, as drawn with a red line in Fig. 6(b). In accordance with the characteristics of endothelial regulation, the pressure pulsatile period was set as 50 s, and the pressure pulsatile amplitude was adjusted to create temperature fluctuation amplitude in the order of  $10^{-3}^{\circ}\text{C}$ . Fixed pressure condition was still set at the four exits of the capillary network, whose values are 33.75 mmHg. To compare temperature fluctuations at different positions, three nodes (X1, X2 and X3) were extracted and their temperature variation curves were drawn in Fig. 6(b). The fluctuation characteristics, including fluctuation amplitude and time delay relative to the inlet blood pressure are listed in Tab. 1, it is found that the temperature fluctuation amplitude is attenuated ( $\Delta T_1 > \Delta T_3 > \Delta T_2$ ) and the time delay is increased ( $\Delta t_1 < \Delta t_3 < \Delta t_2$ ) as the thermal wave propagated in the tissue, which exactly correlate with the distance from the three nodes to the nearest capillary branch ( $d_1 < d_3 < d_2$ ).

**3.3 The influence of the connectivity of capillary network on thermal wave propagation**

It was observed that capillary density was diminished in diabetic microcirculation, and capillaries with micro size even shrink away, which changes the connectivity of a capillary network [Benedict, Coffin, Barrett et al. (2011)]. The capacity of blood redistribution may be altered when the connectivity of capillary network is impaired. To investigate the influence of capillary connectivity on blood redistribution and thermal wave propagation in tissue, a capillary network with impaired connectivity was constructed artificially, where four cross-connecting branches (capillary Nos. 6, 9, 10, 13) were eliminated from the normal case. Compared with other capillaries, the lengths of

these four branches are relatively short and the axial directions are generally perpendicular to the flow directions. Thus, they may act as the role of cross-connecting. Meanwhile, the four entrances (capillary Nos. 12, 17, 18, 24) were obstructed, and the periodical pulsatile pressure was set only at one entrance (capillary No. 23) to study if the network can redistribute blood evenly or not. Fig 7(a) gives the normal capillary network with 4 occluded inlets and Fig. 7(c) is the capillary network with impaired cross-connecting branches at the condition with 4 inlets occluded.

From the distributed blood flow shown in Figs. 7(b) and (d), we found that the capillary network with impaired connectivity was more sensitive to the entrance obstruction conditions. In other words, the capacity of blood redistribution through the capillary network with impaired connectivity becomes weaker. It is seen that when four entrances are obstructed, more than half of the capillary branches lose blood flow, which are expressed in black dotted lines in Fig. 7(d).

Meanwhile, as seen in Fig. 7(d), the tissue temperatures near the occluded entrances are distinctly lower than those in other region, implying that the network with impaired connectivity leads to much lower tissue temperatures. The temperatures of the two nodes at the skin surface (X2 and X3) for the two cases were extracted and are listed in Tab. 2. It is seen that the fluctuation amplitudes of temperature at X2 and X3 are 0.0014 and 0.0018°C respectively for the normal network and further decrease to be 0.0010 and 0.0011°C for the impaired one when the four entrances are occluded. The time delays of the temperature at the two points are larger for the impaired one. The results indicate that amplitude attenuation and time delay of the temperature fluctuation become more serious for the capillary network with the impaired connectivity. Smirnova et al. [Smirnova, Podtaev, Mizeva et al. (2013)] carried out an experiment to measure fingertip temperature variation during a cold pressor test and performed wavelet analyses for the temperature oscillation. It was found that the response to the cold pressor test in patients with type 2 diabetes and with impaired glucose tolerance differs essentially from that of healthy subjects in the endothelial frequency range. Our simulated results give clear reasons for causing the weaker temperature oscillation and larger phase delay.

**Table 2:** Temperature fluctuation characteristics at different tissue nodes after entrance obstruction

Node	Fluctuation amplitude ( $\Delta T$ ), °C	Time delay ( $\Delta t$ ), s
X2 (Normal network)	0.0014	7.5
X2 (Network with impaired connectivity)	0.0010	8.4
X3 (Normal network)	0.0018	7.2
X3 (Network with impaired connectivity)	0.0011	8.4

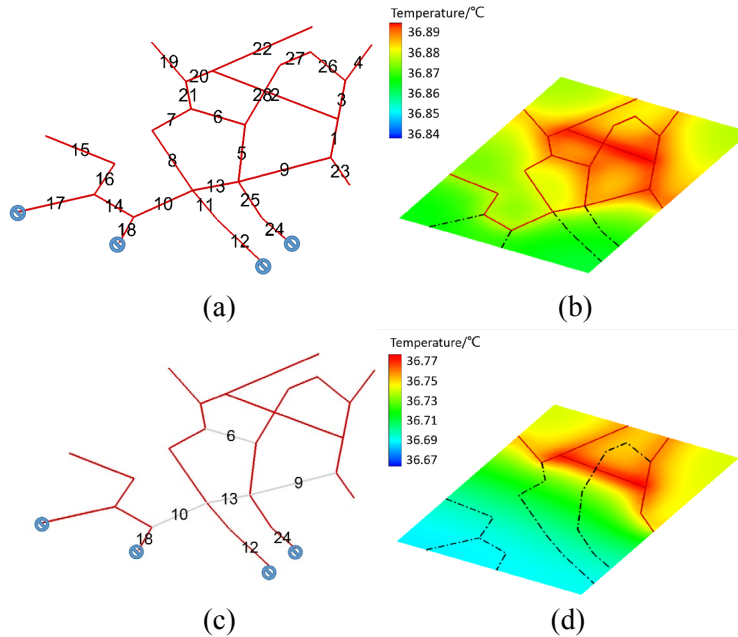


**Figure 7:** Temperature distributions for different vascular structures at the condition of the entrance obstruction. (a) Normal network structure with 4 occluded inlets; (b) Temperature distribution at the plane with the normal capillary network; (c) Impaired capillary network with 4 occluded inlets; (d) Temperature distribution at the plane with impaired capillary network

**4. Conclusions**

In this paper, a model of fluid flow and heat transfer in biological tissue containing the exact microvascular network structure was developed. The capillary network was simplified as a 1D pipeline model and embedded into the extravascular region, which can contribute to the reduction of computational costs by multi-scale modeling of the two sub-domains. The interplay of fluid transport and heat exchange between the capillary network and interstitial tissue was described by IBM. According to the concept of IBM, fluid and heat flux across the capillary wall were distributed to the surrounding tissue nodes by delta function.

Using this model, we simulated thermal wave propagation in tissue. Amplitude attenuation and time delay of temperature fluctuation were found as they propagated. When the perfusions of some capillary branches are lost under the entrance obstruction conditions, skin temperature fluctuations become weaker, especially for the capillary network with impaired connectivity. The findings provide insights into how to use temperature oscillation for evaluation of microcirculation function.

Currently the computation is limited within a highly small region, but it can be easily extended to a larger scale. Meanwhile, the capillary network with impaired connectivity was made artificially. Another work by Wang et al. [Wang, Tang and He (2019)] has confirmed that some branches may be lack of red blood cells when the rheological

behaviors of RBCs are changed. By using the real geometry of microvessel network for a diabetic rat in the model, the relationship between skin temperature and blood flow at diabetic condition will be clearer.

This study shows that IBM can be extended into solving heat transfer problems of biological tissue with complex microvascular network. Although complete 3D modeling for heat transfer in microcirculation is feasible by using an excellent commercial software, the embedded multiscale modeling strategy exhibits a rather general and flexible framework to address the influence of blood flow on heat transfer in biological tissues. It is believed that the modeling method will show more advantages in evaluating heat transfer at pathological conditions and has potential applications in early diagnoses of vascular complications and targeted treatment of tumor.

**Acknowledgement:** This study was supported by National Natural Science Foundation of China (NSFC No. 51576033), Dalian Innovative Funding of Science and Technology (2018J12SN076), and NSFC No 11602053.

**Conflicts of Interest:** The authors declare that they have no conflicts of interest to report regarding the present study.

## References

- Arthurs, K. M.; Moore, L. C.; Peskin, C. S.; Pitman, E. B.; Layton, H. E. (1998): Modeling arteriolar flow and mass transport using the immersed boundary method. *Journal of Computational Physics*, vol. 147, pp. 402-440.
- Astefanoaei, I.; Dumitru, I.; Stancu, A.; Chiriac, H. (2014): A thermo-fluid analysis in magnetic hyperthermia. *Chinese Physics B*, vol. 23, no. 4, pp. 044401.
- Benedict, K. F.; Coffin, G. S.; Barrett, E. J.; Skalak, T. C. (2011): Hemodynamic systems analysis of capillary network remodeling during the progression of type 2 diabetes. *Microcirculation*, vol. 18, no. 1, pp. 63-73.
- Bracic, M.; Stefanovska, A. (1998): Wavelet-based analysis of human blood-flow dynamics. *Bulletin of Mathematical Biology*, vol. 60, no. 5, pp. 919-935.
- Cattaneo, L.; Zunino, P. (2014): Computational models for fluid exchange between microcirculation and tissue interstitium. *Networks & Heterogeneous Media*, vol. 9, no. 1, pp. 135-159.
- Dang, S. N.; Xue, H. J.; Zhang, X. Y.; Qu, Y.; Zhong, C. W. et al. (2018): Three-dimensional human thermoregulation model based on pulsatile blood flow and heating mechanism. *Chinese Physics B*, vol. 27, no. 11, pp. 282-292.
- Frick, P.; Mizeva, I.; Podtaev, S. (2015): Skin temperature variations as a tracer of microvessel tone. *Biomedical Signal Processing and Control*, no. 21, pp. 1-7.
- Gao, T.; Lu, X. Y. (2008): Insect normal hovering flight in ground effect. *Physics of Fluids*, vol. 20, no. 8, pp. 087101.
- Ghafari, A.; Hassanzadeh, A. (2017): Numerical study of red blood cell motion and

deformation through a microchannel using lattice Boltzmann-immersed boundary method. *Journal of the Brazilian Society of Mechanical Sciences and Engineering*, vol. 39, no. 6, pp. 1873-1882.

**Hassanzadeh, A.; Pourmahmoud, N.; Dadvand, A.** (2017): Numerical simulation of motion and deformation of healthy and sick red blood cell through a constricted vessel using hybrid lattice Boltzmann-immersed boundary method. *Computer Methods in Biomechanics and Biomedical Engineering*, vol. 20, no. 7, pp. 737-749.

**Hassanzadeh, A.; Pourmahmoud, N.; Dadvand, A.** (2019): Numerical study of elastic red blood cell motion and deformation using improved Lattice Boltzmann-immersed boundary method. *Iranian Journal of Science and Technology, Transactions of Mechanics Engineering*, no. 43, pp. 57-73.

**Jiji, L. M.; Weinbaum, S.; Lemons, D. E.** (1984): Theory and experiment for the effect of vascular microstructure on surface tissue heat transfer-part II: model formulation and solution. *Journal of Biomechanical Engineering*, vol. 106, no. 4, pp. 331-341.

**Klinger, H. G.** (1974): Heat transfer in perfused biological tissue-I: general theory. *Bulletin of Mathematical Biology*, vol. 36, no. 4, pp. 403-415.

**Krüger, T.** (2012): Computer simulation study of collective phenomena in dense suspensions of red blood cells under shear (*Ph.D. Thesis*). Ruhr-Universität Bochum, Bochum, Germany.

**Liu, W. K.; Kim, D. W.; Tang, S. Q.** (2007): Mathematical foundations of the immersed finite element method. *Computational Mechanics*, vol. 39, no. 3, pp. 211-222.

**Mei, R.; Yu, D.; Shyy, W.; Luo, L. S.** (2002): Force evaluation in the lattice Boltzmann method involving curved geometry. *Physical Review E*, vol. 65, no. 4, pp. 041203.

**Nakayama, A.; Kuwahara, F.** (2008): A general bioheat transfer model based on the theory of porous media. *International Journal of Heat & Mass Transfer*, vol. 51, no. 11-12, pp. 3190-3199.

**Parshakov, A.; Zubareva, N.; Podtaev, S.; Frick, P.** (2017): Local heating test for detection of microcirculation abnormalities in patients with diabetes-related foot complications. *Advances in Skin & Wound Care*, vol. 30, no. 4, pp. 158-166.

**Pennes, H. H.** (1984): Analysis of tissue and arterial blood temperatures in the resting human forearm. *Journal of Applied Physiology*, vol. 1, no. 2, pp. 93-122.

**Peskin, C. S.** (1972): Flow patterns around heart valves: a numerical method. *Journal of Computational Physics*, vol. 10, no. 2, pp. 252-271.

**Peskin, C. S.** (2002): The immersed boundary method. *Acta Numerica*, no. 11, pp. 479-517.

**Pozrikidis, C.** (2010): Numerical simulation of blood and interstitial flow through a solid tumor. *Journal of Mathematical Biology*, vol. 60, no. 1, pp. 75-94.

**Rosis, A. D.; Ubertini, S.; Ubertini, F.** (2014): A comparison between the interpolated bounce-back scheme and the immersed boundary method to treat solid boundary conditions for laminar flows in the Lattice Boltzmann framework. *Journal of Scientific Computing*, vol. 61, no. 3, pp. 477-489.

**Sagaidachnyi, A. A.; Skripal, A. V.; Fomin, A. V.; Usanov, D. A.** (2014): Determination of the amplitude and phase relationships between oscillations in skin temperature and

photoplethysmography-measured blood flow in fingertips. *Physiological Measurement*, vol. 35, no. 2, pp. 153-166.

**Sagaidachnyi, A. A.; Fomin, A. V.; Usanov, D. A.** (2017): Thermography-based blood flow imaging in human skin of the hands and feet: a spectral filtering approach. *Physiological Measurement*, no. 38, pp. 272-288.

**Salloum, M.; Ghaddar, N.; Ghali, K.** (2007): A new transient bioheat model of the human body and its integration to clothing models. *International Journal of Thermal Sciences*, vol. 46, no. 4, pp. 371-384.

**Secomb, T. W.** (1993): Microvascular network structures.

<http://physiology.arizona.edu/people/secomb/network>.

**Shipley, R. J.; Chapman, S. J.** (2010): Multiscale modelling of fluid and drug transport in vascular tumours. *Bulletin of Mathematical Biology*, vol. 72, no. 6, pp. 1464-1491.

**Smirnova, E.; Podtaev, S.; Mizeva, I.; Loran, E.** (2013): Assessment of endothelial dysfunction in patients with impaired glucose tolerance during a cold pressor test. *Diabetes & Vascular Disease Research*, vol. 10, no. 6, pp. 489-497.

**Tang, Y. L.; Mizeva, I.; He, Y.** (2016): A modeling study on the influence of blood flow regulation on skin temperature pulsations. *Saratov Fall Meeting, Proceedings of SPIE*, vol. 10337:1033716, pp. 1-7.

**Tang, Y. L.; He, Y.; Shao, H. W.; Ji, C. J.** (2016): Assessment of comfortable clothing thermal resistance using a multi-scale human thermoregulatory model. *Journal of Heat and Mass Transfer*, no. 98, pp. 568-583.

**Tian, F. B.; Luo, H. X.; Zhu, L. D.; Liao, J. C. et al.** (2011): An efficient immersed boundary-lattice Boltzmann method for the hydrodynamic interaction of elastic filaments, *Journal of Computational Physics*, vol. 230, no. 19, pp. 7266-7283.

**Wang, Y. P.; Tang, Y. L.; He, Y.** (2019): Numerical simulation of the influence of red blood cell distribution on oxygen transport in the capillary network and surrounding tissue. *Proceedings of 6th International Conference on Computational & Mathematical Biomedicine and Engineering*, Sendai, Jun. 10-12, pp. 438-441.

**Wei, J. H.; Song, H.; Shen, Z. Y.; He, Y.; Xu, X. Z. et al.** (2015): Numerical study of pillar shapes in deterministic lateral displacement arrays for spherical particle separation, *IEEE Transactions on NanoBioscience*, vol. 14, no. 6, pp. 660-667.

**Wei, Y. J.; Mu, L. Z.; Tang, Y. L.; Shen, Z. Y.; He, Y.** (2019): Computational analysis of nitric oxide biotransport in a microvessel influenced by red blood cells. *Microvascular Research*, no. 125, pp. 103878.

**Wulff, W.** (1994): The energy conservation equation for living tissue. *IEEE Transactions on Biomedical Engineering*, vol. BME-21, no. 6, pp. 494-495.

**Xuan, Y., Roetzel, W.** (1997): Bio-heat equation of human thermal system. *Chemical Engineering & Technology*, vol. 20, no. 4, pp. 268-276.

**Yuan, P.; Yang, C.; Liu, S.** (2014): Temperature analysis of a biological tissue during hyperthermia therapy in the thermal non-equilibrium porous model. *International Journal of Thermal Sciences, Elsevier Masson SAS*, no. 78, pp. 124-131.